Vera C. Rubin Observatory
Systems Engineering

An Interim Report on the On-Sky Commissioning Campaign with LSSTCam

Keith Bechtol

SITCOMTN-170

Latest Revision: 2025-11-20

DRAFT

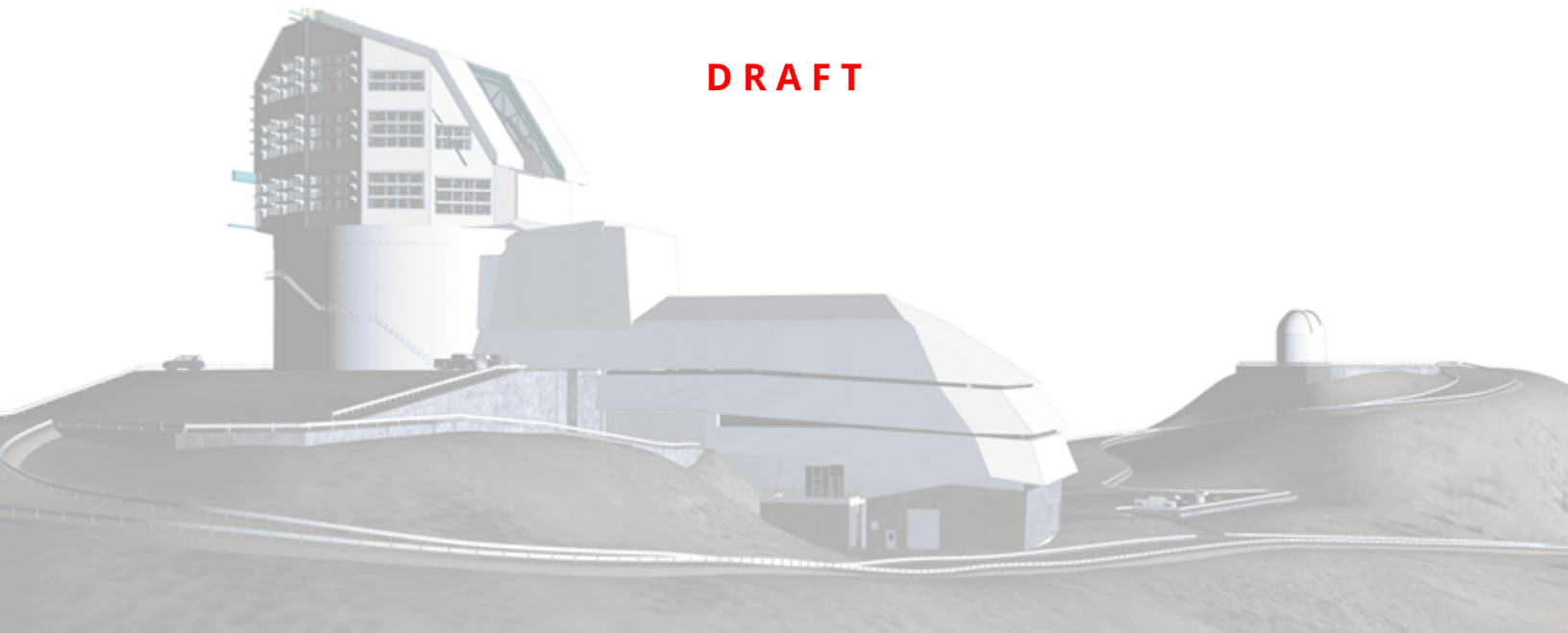

Abstract

From 15 April to 21 September 2025, the NSF-DOE Vera C. Rubin Observatory conducted on an on-sky commissioning campaign using the LSST Camera (LSSTCam) to test the end-to-end functionality of hardware and software, as well as operational procedures. This interim report provides a preliminary technical overview of our understanding of the integrated system performance based tests and analyses conducted during the on-sky commissioning campaign with LSSTCam. The objectives are to synthesize what we have learned about the system in a timely way to inform Early Operations optimization, and to inform the Rubin science community on the progress of the LSSTCam on-sky campaign. The report is organized into sections that describe major activities during the campaign, as well as multiple aspects of the demonstrated system and science performance. All of the results presented here are to be understood as work in progress using engineering data and the initial versions of the data processing pipelines; the report is a living document that will be updated as analyses are refined.

Change Record

Version	Date	Description	Owner name
1	YYYY-MM-DD	Unreleased.	Bechtol

Document source location: `https://github.com/lsst-sitcom/sitcomtn-170`

Contents

An Interim Report on the On-Sky Commissioning Campaign with LSSTCam

1 Introduction

The NSF-DOE Vera C. Rubin Observatory on-sky commissioning campaign using the LSST Camera (hereafter LSSTCam) began on 15 April 2025 and ended on 21 September 2025. This interim report provides a concise summary of our understanding of the integrated system performance based tests and analyses conducted during the LSSTCam on-sky campaign. We seek to distill, and to communicate in a timely way, what we have learned about the system to support the transition from Rubin Observatory Construction to Operations. The report is organized into sections that describe major activities during the campaign, as well as multiple aspects of the demonstrated system and science performance.

Warning: Preliminary Results

All of the results presented here are to be understood as work in progress using engineering data and the initial versions of the data processing pipelines. It is expected at this stage, immediately following the completion of the on-sky commissioning campaign, that several analyses are still in progress, and that some of the discussion will concern open questions, issues, and anomalies that are actively being worked by the team to enhance the system reliability. Additional documentation will be provided as our understanding of the demonstrated performance of the as-built system progresses.

1.1 Charge

Charge Development Historical Note

The initial version of the charge developed in September 2025 is provided below for reference.

We identify the following high-level goals for this interim report:

- **Document our current understanding of the integrated system performance** to support systems engineering verification activities associated with demonstrating Construction Completeness [SITCOMTN-005].
- **Transfer knowledge to support the transition from Construction to Operations** to inform the Early Operations optimization period and to support the Early Science Program [RTN-011].
- **Inform the Rubin Science Community** on the progress of the on-sky commissioning campaign using LSSTCam.

Formal acceptance testing with respect to system-level requirement specifications (LSE-29 and LSE-30) will be recorded using the LSST Verification & Validation (LVV) system. By design, several of the analyses presented in this report correspond to system-level requirements, and therefore, this report is anticipated to serve as a verification artifact to support several of those systems engineering activities.

The groups within the Rubin Observatory project working on each of the activities and performance analyses are charged with contributing to the relevant sections of the report. The anticipated level of detail for the sections ranges from a paragraph up to a page or two of text, depending on the current state of understanding, with **quantitative performance** expressed as summary statistics, tables, and/or figures. The objective for this document is to **summarize the state of knowledge of the system**, rather than how we got there or "lessons learned". The sections refer to additional supporting documentation, e.g., analysis notebooks, other technotes with further detail, as needed. Given the timelines for commissioning various aspects of the system, it is natural that some sections will have more detail than others.

The anticipated milestones for developing this interim report are as follows:

- 18 Sep 2025: Define charge
- 22 Sep 2025: On-sky commissioning campaing with LSSTCam completed; start of final construction downtime and its first operations engineering downtime
- 8 Oct 2025: Detailed outlines with initial versions of essential figures and performance statistics for report sections made available for internal review (content can be on un-

merged development branches); a goal is to help systems engineering with mapping of report content to requirements verification

- 15 Oct 2025: Revised drafts of report sections made available for internal review; development branches merged to main branch; editing for consistency and coherency throughout the report
- 22 Oct 2025: Start of Construction to Operations Transition Workshop; advanced draft ready for review by full Rubin Observatory team
- 31 Oct 2025: Initial version of report is released

2 Executive Summary

Executive summary here.

Versioning Note

This interim report provides a preliminary technical overview of the LSSTCam on-sky campaign based on analyses through October 2025.

2.1 Accomplishments

- **Accomplishment.** Description.
- **Accomplishment.** Description.
- **Accomplishment.** Description.

2.2 Areas of Ongoing Investigation and Further Development

- **Issue.** Description.
- **Issue.** Description.
- **Issue.** Description.

3 Sensor Performance and Instrument Signature Removal

- Usable pixels, effective field of view, fill factor
- Read noise
- Crosstalk
- Dynamic range (brightest and faintest objects)
- Summary table of key Camera performance metrics
- Section needs at least one figure to visualize focal plane; maybe a flat?
- Standard visit (i.e., snaps) evaluation?

We performed comprehensive in-dome calibration to generate calibration products and validate LSSTCam. Calibration data not requiring external illumination included biases and darks. We operated the Flat Field Projector with single-LED flats and generated Photon Transfer Curves (PTCs). We exercised both calibration system sources: a white-light LED with a fiber spectrograph and photodiode plus electrometer, and a tunable laser with the same metrology chain. We used the Collimated Beam Projector (CBP) for filter scans (and no-filter scans) and to acquire crosstalk spot data. These activities validated the calibration pathways and established in-situ sensor performance baselines.

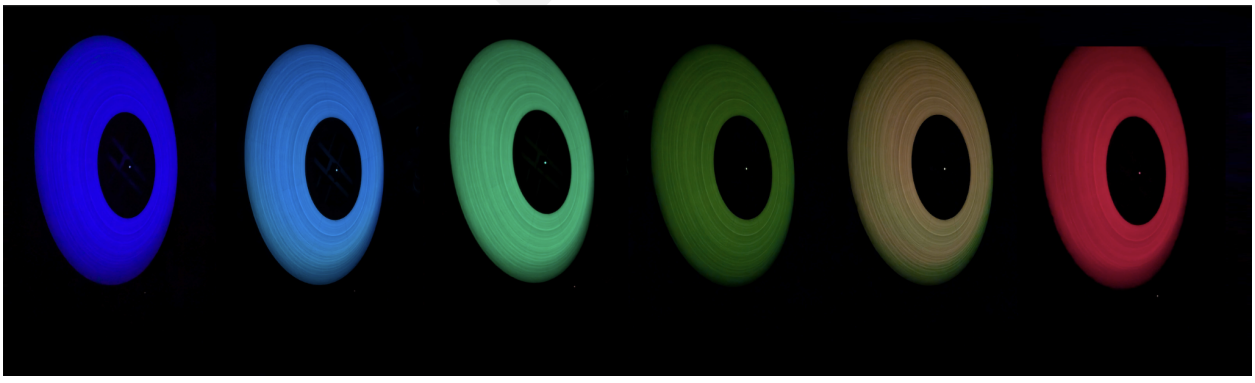

FIGURE 1: Our flat field screen illuminated by our single LEDs and pairs of single LEDs. The LEDs from left to right are named Royal Blue, both Royal Blue and Green, Green, Lime, both Lime and Deep Red, Deep Red)

A total of 188/189 sensors are operational, with only R30/S12 currently non-operational. The median amplifier loses ~0.45% of its area to defects, while the mean across amplifiers is closer

to ∼0.7%. Elevated defect counts appear where effective QE is lower at detector edges, especially for Cy0 and Cy7 amplifiers. No new static defect classes have been identified on e2v devices (hot/cold pixels and columns remain as expected), while a subset of ITL detectors exhibits "vampire" pixels and locally higher noise. Dynamic masking still requires work, including treatment of e2v edge bleeds and occasional flare-type artifacts when bright stars fall on extreme detector edges. Overall, $\gtrsim$99% of the focal plane is active and usable within the calibrated field.

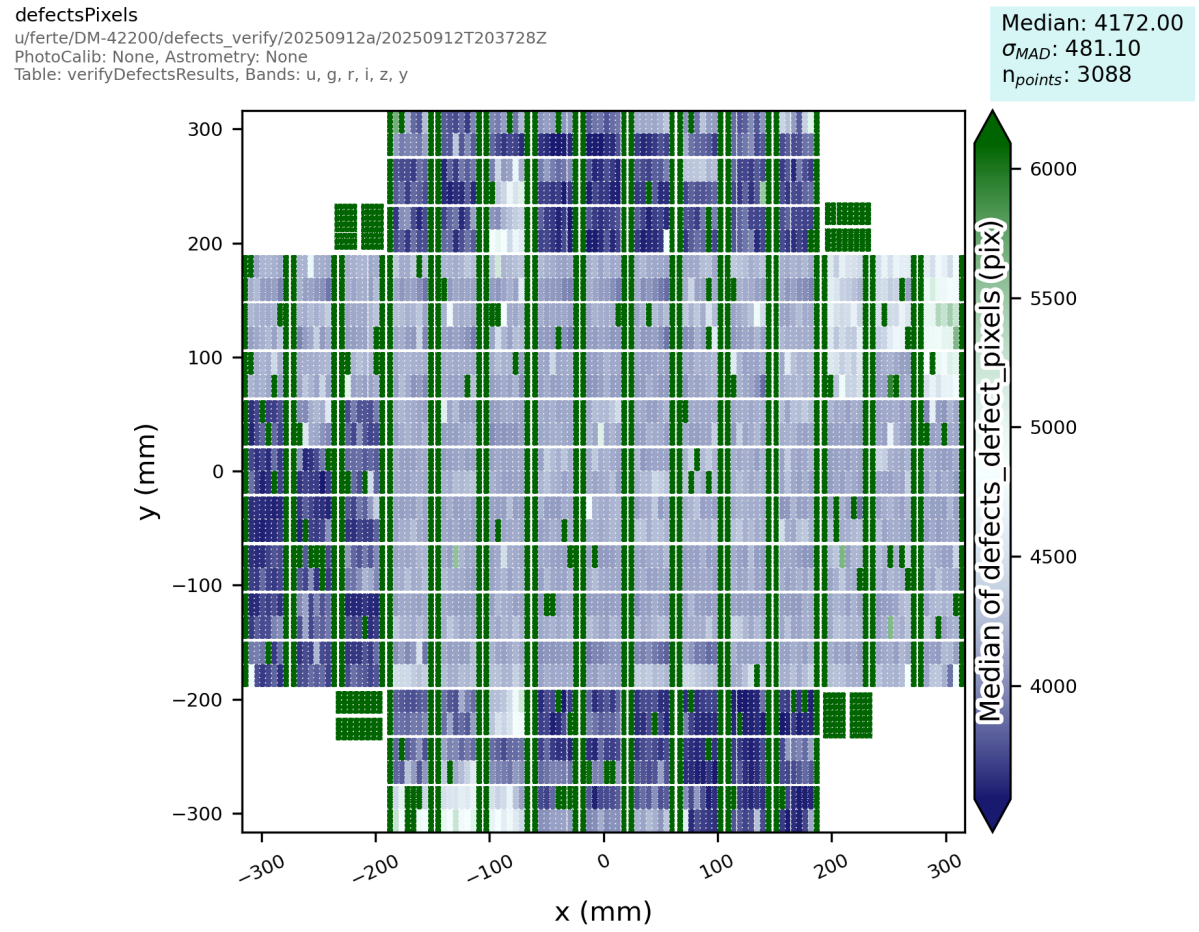

FIGURE 2: Usable pixels summary: 188/189 sensors operational (R30/S12 offline), median amplifier defect area ∼0.45% (mean ∼0.7%), with edge-related QE behavior raising counts in Cy0/Cy7 amplifiers; no new static defect types on e2v, "vampire" pixels seen on some ITL detectors.

Optical vignetting limits the fully calibrate-able radius to the camera requirement of 317 mm (black circle). We introduced a PARTLY_VIGNETTED mask plane for 317–350 mm radius (red circle), where calibration is expected to be feasible but at reduced fidelity relative to the inner zone. If calibration to 350 mm is achieved, the residual loss of area relative to the geometric

maximum radius of 365 mm (blue circle) is minimal, affecting only the extreme corners of the focal plane. Regions outside 350 mm are treated as fully vignetted and excluded from science products.

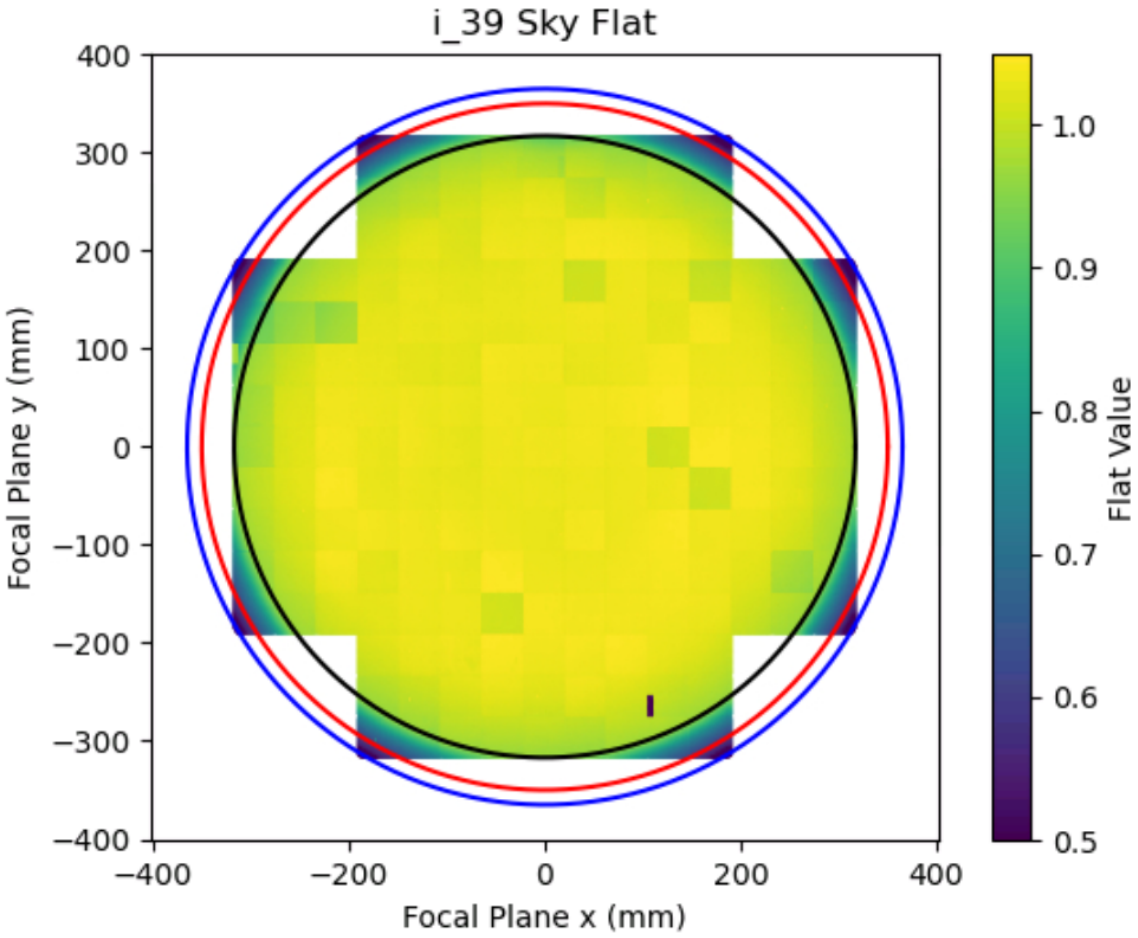

FIGURE 3: Optical vignetting and calibrate-able field of view: requirement radius 317 mm (black), target extension to 350 mm (red) for partial vignetting, and geometric maximum 365 mm (blue).

Read-noise maps show all channels in specification, with ITL devices having slightly higher medians than e2v and some top–bottom amplifier shifts visible on subsets of ITL sensors. Gain maps show nominal values consistent with design and optimal ADC usage. PTC turn-off levels indicate amplifier dynamic ranges typically near $\sim 10^5$ DN, with subsets lower; pixels above the turn-off are saturated in processing. CBP spot data confirm that the updated sequencer reduces noise and correlations, but crosstalk coefficients require re-derivation post-change; first-order terms are largely removed while higher orders remain to be tuned for DP2 processing. No new major anomalies were uncovered during these campaigns, and calibration

improvements are being integrated iteratively into ISR and downstream processing.

3.1 Summary

All calibration systems were exercised end-to-end, and their products validated in dome. :contentReference[oaicite:3]index=3 Operational yield is 188/189 sensors with ≳99% active focal-plane area within the calibrate-able region. :contentReference[oaicite:4]index=4 A `PARTLY_VIGNETTED` mask enables use out to 350 mm radius with controlled fidelity, minimizing area loss to extreme corners while avoiding over-fitting in fully vignetted zones. Read noise, gain, and dynamic range meet expectations, and post-sequencer crosstalk calibration is in progress for DP2.

3.2 Bright Stars and Moon

On-sky validation that the Camera can survey the night sky in the presence of bright sources

3.3 Sensor Anomalies

Any sensor anomalies that are worth noting

3.4 LSSTCam Performance during the LSSTCam On-sky Campaign

Brief summary of LSSTCam performance during the campaign, any open questions, outstanding issues

This could include any discussion on Camera susbsystems, e.g., focal plane optimization, filter exchange system, cryo, camera shutter, that should be highlighted

4 System Optical Throughput for Focused Light

- Standard bandpass; includes the sensors, filters, lenses, mirrors, and (a standard) atmosphere. Measured with CBP? Monochromatic flats with flat field screen?
- Imaging depth in multiple bands (LSR-REQ-0090); also express as zeropoint to separate

out the effects of image quality; could be comparison to refcats and/or spectrophotometric standards

- Figure to show throughput variation of throughput across field of view (LSR-REQ-0109); potentially separating out vignetting and CCD response
- Discussion on Sensitivity Factor (fS) in the System Performance Diagram

4.1 Standard Bandpass

4.2 Measured Zeropoints

5 Measured Sky Backgrounds

During the LSSTCam on-sky campaign, dedicated tests were performed to characterize the background, evaluate the performance of the `SkyCorrectionTask`, and verify compliance with project-level requirements.

5.1 Sky Brightness Determination

Sky brightness measurements were performed using forced photometry on randomly placed "sky sources" across the focal plane. Sky sources are defined as circular apertures with a radius of 8 pixels that avoid detected footprints or regions of bad or missing data. For each sky source position, the local sky flux was compared to the fitted background model prediction. Across the sample of real LSSTCam data, the precision of the sky brightness determination was better than 1% in approximately 99% of all measurements, meeting the system requirement (Fig. 4).

These tests used data from weekly DRP processing runs (e.g., week 18) that employed the full-focal-plane background modeling introduced with the `SkyCorrectionTask`. This task, initially developed for HSC, has been subsequently commissioned for use with LSSTCam. It operates by fitting large sky gradients across the full focal plane, in addition to subtracting the "sky frame"; flux which remains static in focal plane coordinates after all other calibrations have been applied. Comparisons between per-detector and full-focal-plane background solutions show that the latter reduces over-subtraction near bright, extended sources and improves uniformity across the field.

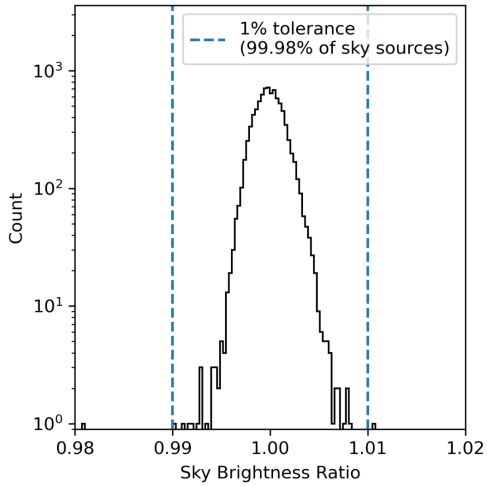

FIGURE 4: Performance of sky brightness determination using forced photometry of randomly placed sky sources. Nearly all measurements (∼99%) achieve better than 1% precision, satisfying the system requirement.

5.2 Limiting Surface Brightness Sensitivity

Random sampling of sky regions from ten representative g-band LSSTCam visits yields a limiting surface brightness of ∼28 mag arcsec^{-2}. This limit is defined as three times the standard deviation of the background flux distribution within 10 arcsecond boxes. Further validation using LSSTComCam radial photometry of the brightest cluster galaxy (BCG) in Abell 360 confirms that surface brightness features are detected to similar levels in multiple bands (Zhou et al., SITCOMTN-165, SITCOMTN-165). These measurements demonstrate that the system is achieving the expected depth for extended, low surface brightness structures (Fig. 5).

5.3 Optical Ghost Area Impact

Optical ghosts have the potential to impact the effective background by contaminating large sections of any given exposure. Using the `Batoid` optical model ray-tracing software calibrated to observed LSSTCam data, we quantify the loss of usable imaging area due to ghosting.

5.3.1 Simulation Scheme

Bright stars from the Yale Bright Star Catalog were queried for each LSSTCam visit and their magnitudes transformed from V-band to LSST magnitudes using a set of transformation equa-

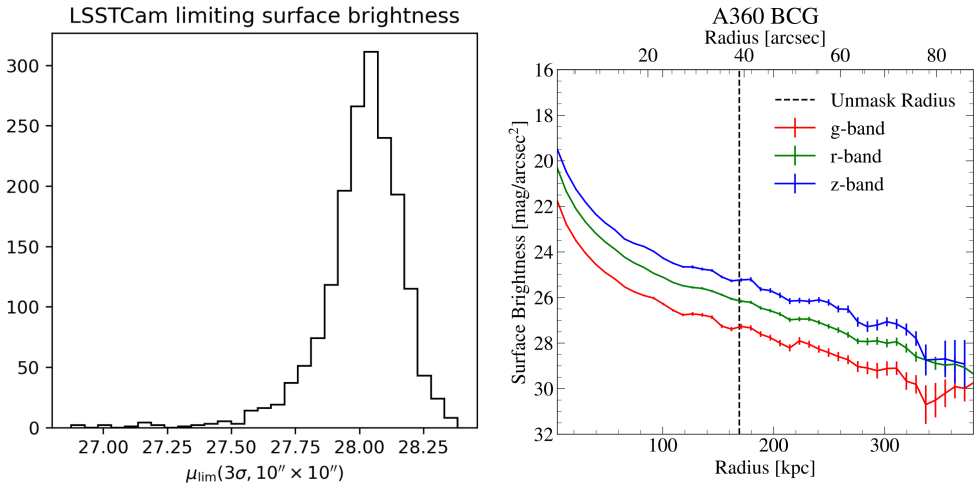

FIGURE 5: Low surface brightness performance. *Left:* Random sampling of g-band LSSTCam visits yields a limiting surface brightness of ∼28 mag arcsec^{-2}. *Right:* LSSTComCam Radial photometry around the BCG in Abell 360 confirms consistent surface brightness sensitivity across filters.

tions derived from the MONSTER reference catalog (Ferguson et al., DMTN-277, DMTN-277). In addition to V-band magnitudes, transformations also rely on the reported B-V color of the stars. Using their reported coordinates, each star is then initialized into a Batoid ray-tracing simulation with the reflectances of the simulated optical elements set to the values produced by systems engineering simulations in the `syseng_throughputs` package.

The rays were propagated through the full system to produce simulated optical ghosts across an entire exposure. A ghost was considered to be "significantly impacting" if the surface brightness of the ghost (in counts per pixel) was greater than 1/3 of the median sky noise (estimated from the data for each visit) in at least one of the detectors. The procedure is shown in detail in Pai (SITCOMTN-173).

5.3.2 Impacted Area Statistics

The week 37 DRP dataset (`LSSTCam/runs/DRP/20250604_20250906/w_2025_37/DM-52496`) was used as a proxy to assess the expected area impacted by optical ghosts in LSST during operations. The DRP contains ∼3100 visits on which to assess ghost area impact. The top panel of Fig. 7 (cyan points) shows that the typical "usual case" average ghost-affected area is ∼0.6% when averaged across all bands. The average ghost-affected area is highest in u and lowest in r and i. This satisfies the nominal system requirement that the fractional area impacted by ghosts

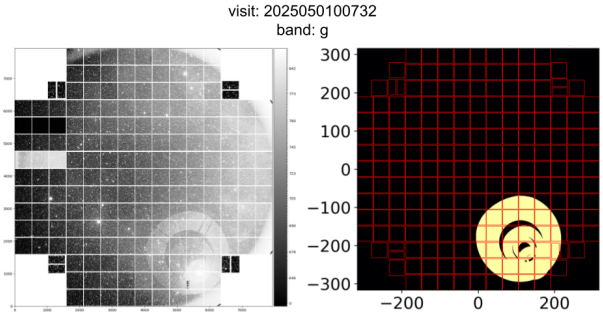

FIGURE 6: Left: An example of ghosting in LSSTCam visit 2025050100732, with ghosting evident in the bottom-right corner of the focal plane. Right: The area found to be significantly impacted by ghost artifacts highlighted in yellow, as determined using a `Batoid` simulation of the bright star in the image.

remain below 1%.

As expected, the ghost area impact is highly dependent on the fields being observed. To assess the variation in the ghost-affected area, 20 highly-ghosted visits were selected in each band[1] by visual inspection which serve as the "worst case" impacted area. As shown, the worst case ghost area impact is highest in u at ∼8%, dropping to below 1% in z.

The total ghost impacted area was also calculated as a function of star magnitude in each band by placing simulated stars at different off-axis positions within the focal plane. The bottom panels in Fig. 7 show the fraction of the focal plane impacted as a function of simulated LSST star magnitude, for both on-axis in multiple filters (left panel) and off-axis in the r band (right panel). As shown here, the impacted area does not appear to depend strongly on field position, with star magnitude the dominant factor as expected.

5.4 Summary

The commissioning campaign demonstrated that LSSTCam background modeling meets or exceeds requirements. Sky brightness precision is better than 1%, limiting surface brightness sensitivity reaches ∼28 mag arcsec^{-2}, and the fractional area affected by optical ghosts remains below 1%. These results validate both the photometric and low surface brightness performance of the system and establish a foundation for continued optimization of background modeling in future data releases.

[1] except in the y band, for which 20 example visits with severe ghosting could not be identified.

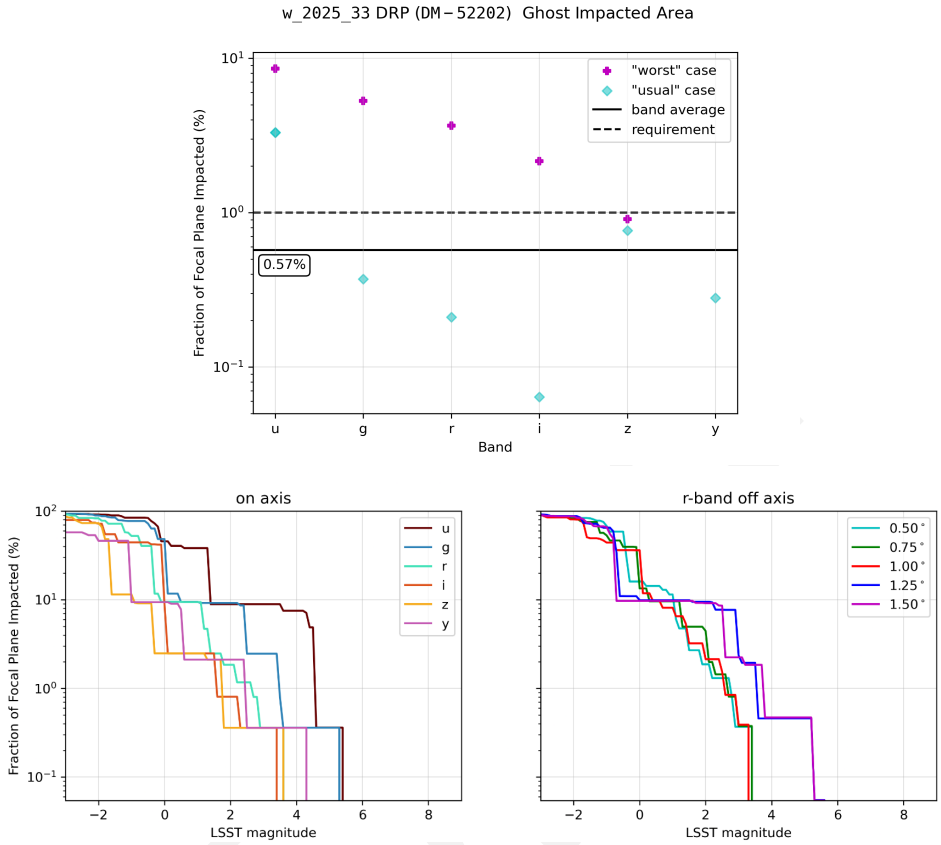

FIGURE 7: (Top) Fraction of the focal plane impacted by optical ghosts simulated with `Batoid` as a function of bandpass. The "usual case" impacted area values (cyan diamonds) are calculated using visits from a recent DRP data reduction run designed to mimic data taken during operations while the "worst case" impacted area values (purple crosses) are calculated using visits that contain high amounts of ghosting selected by visual inspection. The average impacted area across all bands is ~0.6%, with the most area lost in u and least in r and i, satisfying the requirement that ghost area loss remain below 1%. (Bottom Left) Impacted area as a function of on-axis simulated star magnitude in each band. (Bottom Right) Impacted area as a function of field position of the simulated star in the r-band. The impacted area does not vary heavily with field position, with star magnitude the dominant factor.

6 Delivered Image Quality

6.1 Delivered Image Quality Distribution

- Examples of some of our best images to demonstrate system capability
- Figure: distribution of PSF FWHM for an ensemble of visits
- Figure: PSF size and ellipticity distribution across field of view for an ensemble of visits

6.2 Image Quality Budget

Discussion on current assessment of the various contributions to the delivered image quality, accomplishments, open questions, outstanding issues

Discussion on current state of characterizing the atmosphere contribution

6.3 PSF Characterization

The characterization of the point spread function (PSF) provides a key measure of the image quality and calibration performance achieved during LSSTCam commissioning.

6.3.1 Focal Plane Residuals

Average PSF size residuals across the focal plane are at or below the 0.5% level, indicating sub-percent accuracy in the PSF modeling (Fig. 8). When the residuals are stacked across ensemble visits, distinct spatial structures become visible. A ring-like pattern at the edge of the field corresponds to vignetting effects. Small amplifier-level offsets are observed on e2v sensors. Most notably, a "blob" pattern appears on ITL sensors, consisting of circular features within each device.

These ITL features are highly correlated with the height map of each sensor measured during laboratory testing at SLAC. (Fig. 9). Blink comparisons between the PSF residual maps and the measured height maps show an excellent correspondence. This confirms that local defocus from sensor height variations produces the observed PSF structure. The PSF thus serves as a secondary map of focal-plane topography, which can be incorporated into future models to further reduce residuals.

6.3.2 Brighter–Fatter Correction

The dependence of PSF size on source flux—the brighter–fatter effect—has been modeled and corrected using an electrostatic approach. This new model achieves accuracy better than 0.5%, satisfying and exceeding both Rubin internal requirements and external dark-energy science goals. Comparisons of residual PSF size as a function of flux show that the electrostatic model removes the previous over-correction observed in the default pipeline. Implementa-

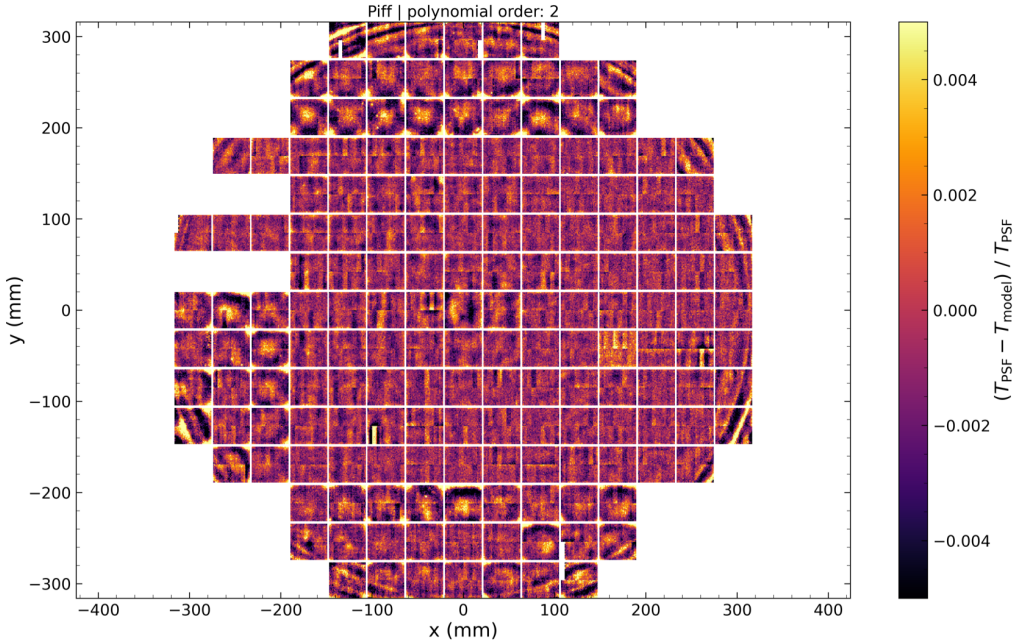

FIGURE 8: Average PSF size residuals across the LSSTCam focal plane. Residuals are at the ≤0.5% level. The ring at the edge corresponds to vignetting, small offsets appear on e2v sensors, and the blob pattern on ITL sensors matches the laboratory-measured sensor height map from SLAC.

tion of this improved correction in standard processing is in progress.

6.3.3 Ongoing and Future Work

Several enhancements to PSF modeling are under active development. A chromatic PSF model has been demonstrated and implemented in the pipeline but is not yet enabled by default. Work is underway to transition from per-CCD to full focal plane PSF modeling. Efforts are also in progress to shift from pixel coordinates to sky coordinates for PSF interpolation and to incorporate laboratory-measured sensor height information directly into the model. Each of these improvements is expected to further reduce PSF residuals and improve astrometric and shear accuracy.

PSF characterization during LSSTCam commissioning demonstrates that the system achieves sub-percent modeling accuracy across the focal plane. Residual patterns correlate strongly with known sensor characteristics, validating both the physical understanding and calibration

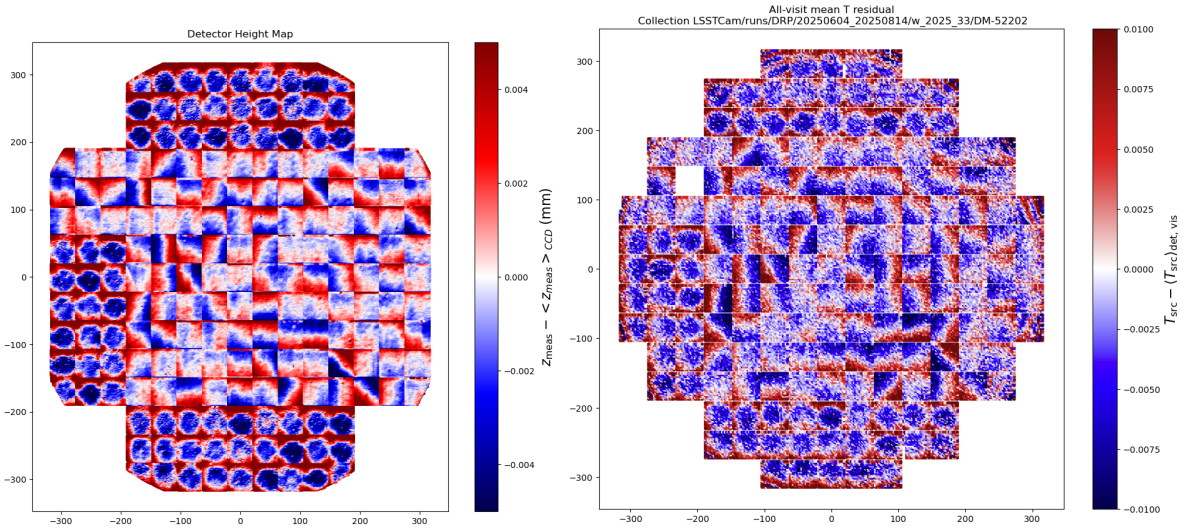

FIGURE 9: Size residuals are highly correlated with the laboratory-measured sensor height map from SLAC.

fidelity of the system. With the inclusion of chromatic and full-focal-plane models in upcoming releases, PSF performance is expected to reach the design specifications required for precision cosmology.

7 Stray and Scattered Light

The unique, wide-field design of the Simonyi Survey Telescope makes it particularly susceptible to stray and scattered light. Since LSST seeks to investigate the low-surface-brightness universe (Ivezić et al., 2019), it is important to identify, model, and mitigate stray-light artifacts. This is particularly important in the context of the delayed installation of the light–wind screen (LWS; Marchiori et al., 2024). A general overview of the investigation of stray light features during commissioning can be found in Rodeghiero (SITCOMTN-160), while a detailed investigation of the most prominent stray light feature (the "scratched tape") is discussed in Drlica-Wagner et al. (SITCOMTN-166). Here, we provide a brief summary of those efforts and the impact of stray and scattered light.

A diverse set of stray and scattered light features were identified during the LSSTCam commissioning campaign. In contrast to optical ghosts, which are expected due to reflections within the optical system, stray and scattered light artifacts arise from unwanted light paths that do not follow the designed optical train. They include parasitic illumination that reaches the focal

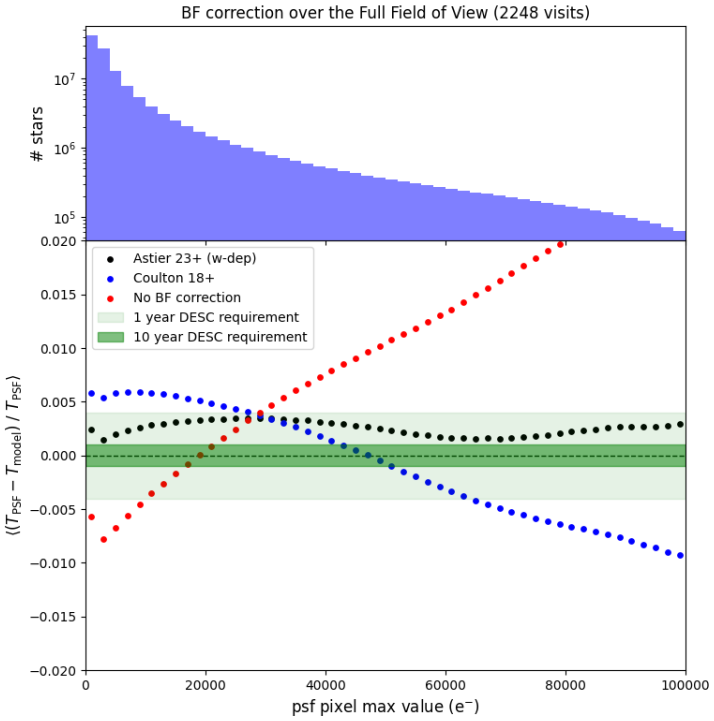

FIGURE 10: Brighter–fatter correction performance. The blue curve shows the uncorrected flux-dependent PSF size residuals, the red curve the current pipeline correction, and the black curve the new electrostatic model. The latter achieves sub-0.5% accuracy and removes the over-correction seen previously.

plane through reflections, scattering, or incomplete baffling of external light sources.

To date, more than a dozen distinct stray-light features have been cataloged. The team has determined the optical or opto-mechanical origin for several of these features, while others remain under investigation. Most of the remaining unidentified features are expected to be mitigated by the LWS, which is expected to become fully operational in the coming months. In addition, other mitigations strategies have been pursued including extra baffling and reduction of in-dome light sources.

7.1 Identification and Characterization

The process of identifying, investigating, and characterizing stray and scattered light artifacts proceeded in several steps. The order in which these steps were executed varied from feature to feature.

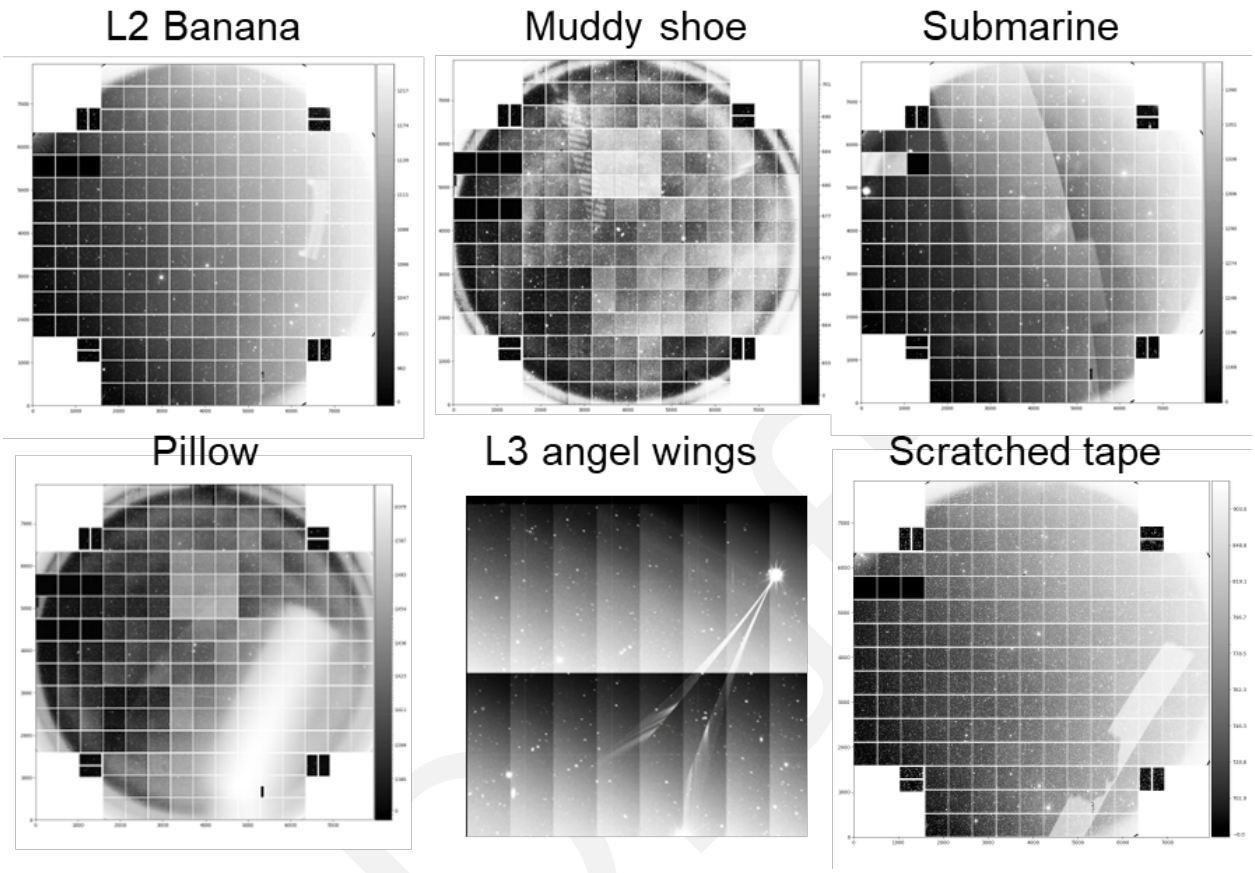

FIGURE 11: Examples of stray and scattered light features observed during LSSTCam commissioning. More than a dozen artifacts have been cataloged. Several of the most prominent artifacts have been traced to specific opto-mechanical origins. The incidence of stray and scattered light artifacts are expected to be significantly mitigated by the Light Wind Screen and additional baffling improvements.

1. **Identification:** Systematic visual inspection of post-ISR-processed LSSTCam images was performed throughout commissioning. When new stray light features were identified, they were circulated among a team of experts for discussion.

2. **Classification and Documentation:** Artifacts were compared to a library of known artifacts to determine whether they represents a novel feature.

3. **Modeling and Reproduction:** Optical ray tracing was performed (i.e., using `Zemax` and `Batoid`) to reproduce the observed geometry and intensity distribution.

4. **On-Sky and In-Dome Testing:** Dedicated test observations were performed to confirm or better understand the source and optical path. These observations included on-sky and in-dome images. The CBP was used to provide specific illumination paths during

in-dome testing.

5. **Source Identification:** Carry out astrometric searches to locate the bright astronomical source (star, planet, or the moon) responsible for generating the feature.
6. **Mitigation Assessment:** Evaluate hardware and operational mitigations, including additional baffling, surface treatment, and observing constraints.
7. **Impact Evaluation:** Estimate the potential scientific impact on photometric and background measurements.

A total of nine hours of on-sky testing (twelve test cases) and fifteen hours of in-dome testing (eight test cases) were dedicated to this effort. Weekly coordination meetings between the stray-light task force and LSSTCam Science Unit have been maintained to ensure progress in both diagnosis and mitigation.

7.2 Example: The "Scratched Tape" Artifact

The most prominent and frequent stray-light feature identified during commissioning is colloquially referred to as *Scratched Tape*. It manifests as a series of bright, elongated streaks across the focal plane (Fig. 12). These features can reach surface brightness levels up to ∼20% of the dark-sky background and appear prominently in roughly 5% of the exposures taken during commissioning. Their structured pattern and relatively high contrast make them among the most visually prominent and scientifically significant artifacts observed.

Through a series of investigations including pinhole imaging, twilight flats, and optical modeling, the origin of the Scratched Tape feature was traced to an unobstructed light path between the mid-level and center-section light baffles on the Telescope Mount Assembly (TMA). Light entering the system at an off-axis range from ∼20 to ∼25 degrees can pass through this gap, reflect off of M1, and scattered directly into the camera. This large off-axis path is expected to be blocked by the Light Wind Screen once it is operating; however, the system was not deployed at the time of commissioning.

In addition to in-dome testing, the feature was also successfully reproduced in targeted on-sky tests by placing a bright star ∼21 degrees off-axis in the identified azimuthal sector. Both `Zemax` and `Batoid` simulations confirmed that an unobstructed light path existed between the

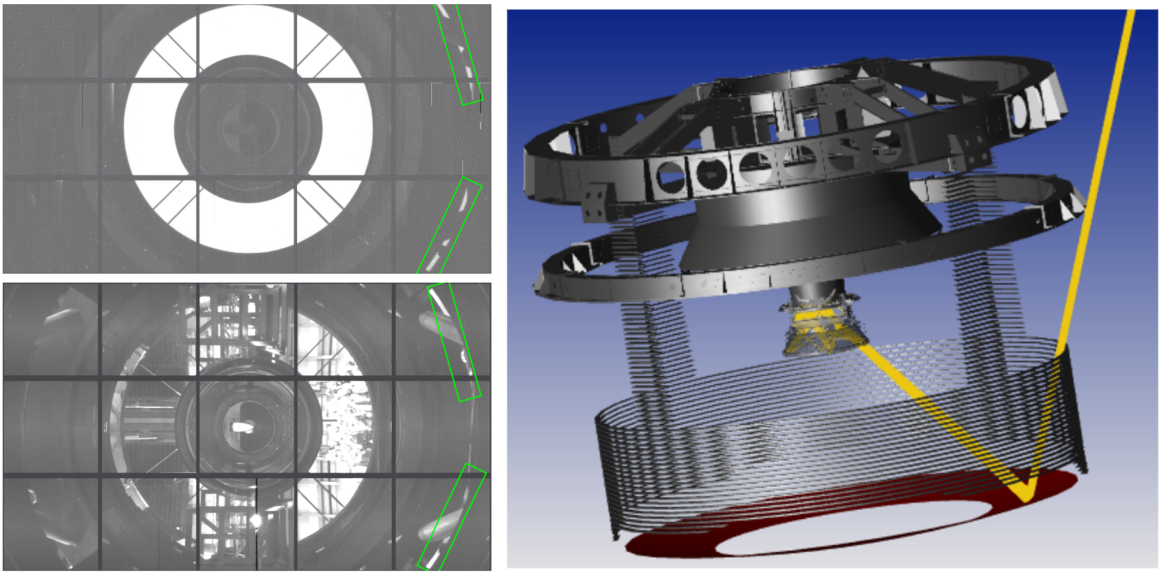

FIGURE 12: Identification of the light path responsible for the "Scratched Tape" artifact. *Left:* pinhole images taken on-sky during twilight (top) and in-dome (bottom). The unbaffled light path between the TMA mid-level and center-section baffles is identified with green boxes. *Right:* modeling in confirmed the existence of a direct off-axis light path through this gap, off of M1, and into the camera. Figure adapted from Drlica-Wagner et al. (SITCOMTN-166).

two baffles that could illuminate the camera. Independent tests with the CBP verified the same geometry under controlled dome conditions.

7.3 Short-term Mitigation Plan

It is suspected that several of the stray light features identified during commissioning may come from similar unobstructed paths at high off-axis angles, since much of the TMA and camera baffling was not designed with such a large incident angle range in mind. Eventually these light paths are expected to be blocked by the Light Wind Screen. However, in the stort term, an effective mitigation strategy is to extend the mid-level baffle outward by approximately 22 cm. This baffle extension offers a simple, robust, and immediate reduction of the Scratched Tape feature with no expected optical or mechanical drawbacks. The design has been finalized and installation is expected to start in late November.

Following installation, additional on-sky and in-dome tests will be performed to verify that the light path is fully blocked. Further mitigations under study include improving the M2 baffle coating, additional blackening of reflective surfaces near the auto-changer, and evaluation of direct paths from M3 to the camera. In parallel, algorithmic approaches for detecting and

removing residual stray-light features at the data-processing stage are being explored.

7.4 Summary

The investigation of stray and scattered light during LSSTCam commissioning has established a framework for discovering, modeling, and mitigating parasitic optical features affecting the LSSTCam images. Thorough investigations of the most prominent stray light features have resulted in a detailed understanding of their origins and have enabled short- and long-term mitigation strategies. Continued refinement of the opto-mechanical model, expanded baffling, and the commissioning of the Light Wind Screen are expected to significantly reduce stray light in operations.

8 System Timing and Dynamics

- Standard Visit Duration (OSS-REQ-0288)
- Readout time – discussed with the Camera?
- Time Interval Between Visits (OSS-REQ-0289)
- Maximum time for operational filter change (OSS-REQ-0293)
- Telescope Azimuth Slewing Rate (TLS-REQ-0029)
- Telescope Elevation Slewing Rate (TLS-REQ-0159)
- Summative assessment on rate of acquiring observations

8.1 Standard Visit Definition

Discussion on decision to use 30-second exposures

8.2 Visit Timing and Interval between Visits

Camera readout time, filter change times

Telescope motion settings, slew and setttle, distribution of time between visits

8.3 Effective Survey Speed

Observing efficiency factor (fO) for System Performance diagram

Survey simulations combined with telescope motion capabilities; compare with actual rate of acquiring visits during SV surveys

9 Data Management

The primary purpose of this section is to describe that data management has been able to support the operational aspects of running Rubin Observatory during commissioning

- Calibration products and ISR during commissioning
- Brief description (paragraph or two; maybe a table) of data processing campaigns during on-sky commissioning, mainly reporting on the functional capabilities; algorithms and data products are discussed elsewhere; pointers to other references
- Figure with representative pixel-level color coadd images?

10 Calibration

10.1 Astrometry

Astrometric calibration establishes the geometric fidelity of the LSSTCam imaging system and ensures that object positions are consistent across visits and with external reference catalogs. The analysis presented here summarizes the current performance achieved during the Science Validation campaign and identifies the dominant sources of residual error.

10.1.1 Global Calibration

The global astrometric calibration is performed using the `gbdesAstrometricFit` model, which fits for source proper motions and parallaxes across all visits. Differential chromatic refraction (DCR) fitting will be enabled in upcoming processing runs. Recent improvements include the

introduction of multiprocessing and the switch from small tract-level runs to larger HEALPix regions. These changes significantly reduced total processing time and improved overall convergence stability.

The resulting astrometric repeatability meets design expectations in most regions of the sky observed with full focal-plane dithers. Figure 13 shows the AM1 metric, defined as the standard deviation of the separation between pairs of objects approximately five arcminutes apart. Typical values are at the ∼10 milliarcsecond (mas) level, with localized regions showing higher scatter that are under investigation.

10.1.2 Residual Patterns and Atmospheric Contribution

Mean astrometric residuals binned by position in the focal plane are shown in Figure 14. The residuals in both X and Y directions are reveal effects at the chip level. For example the features on the ITL detectors are consistent with the laboratory measured sensor height maps. These higher order distortions remain at the individual chip level and will be modeled out in future iterations.

Because LSSTCam uses relatively short 30-second exposures, atmospheric turbulence introduces correlated position shifts across the field. A Gaussian-process model has been developed to represent this atmospheric component and is being tested for inclusion in the standard pipeline. This model reproduces the observed E-mode correlation structure seen in the residuals and reduces the single-visit scatter by roughly 50% when applied.

After subtraction of the modeled atmospheric term, stacked residual maps reveal additional fine-scale structure, including chip-dependent distortions and faint tree-ring patterns on ITL sensors. These effects are below the atmospheric level but are now detectable due to reduced noise and will be incorporated into refined models.

10.1.3 Refined Camera Distortion Model

Astrometric solutions have been used to derive an updated camera distortion model, replacing the pre-commissioning geometric model from `obs_lsst`. This new model reflects the as-built optical system and the measured alignment of detectors in situ. The difference between the two models is shown in Figure 16. After removing a first-order affine transformation, small

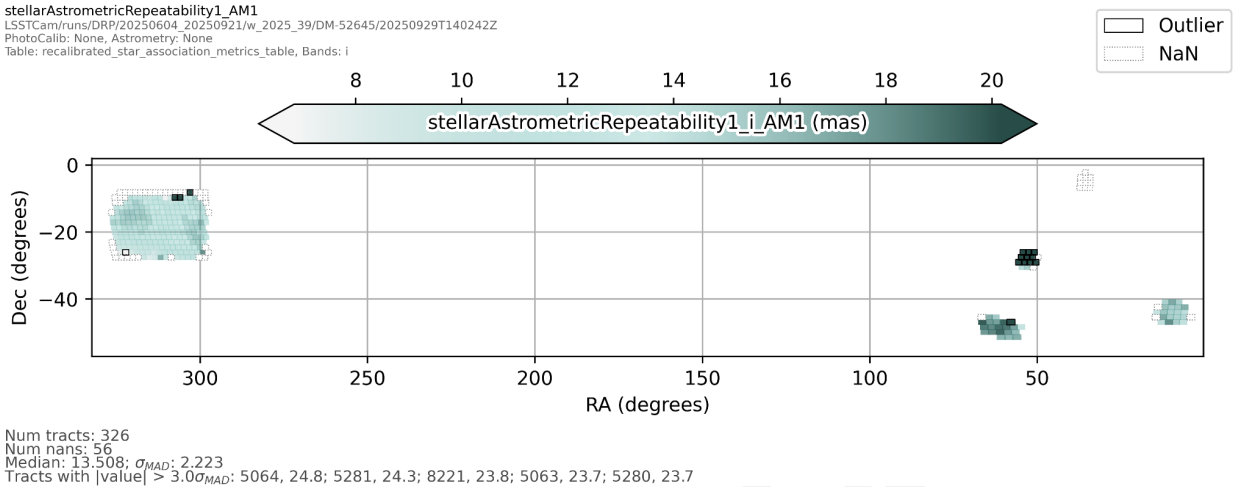

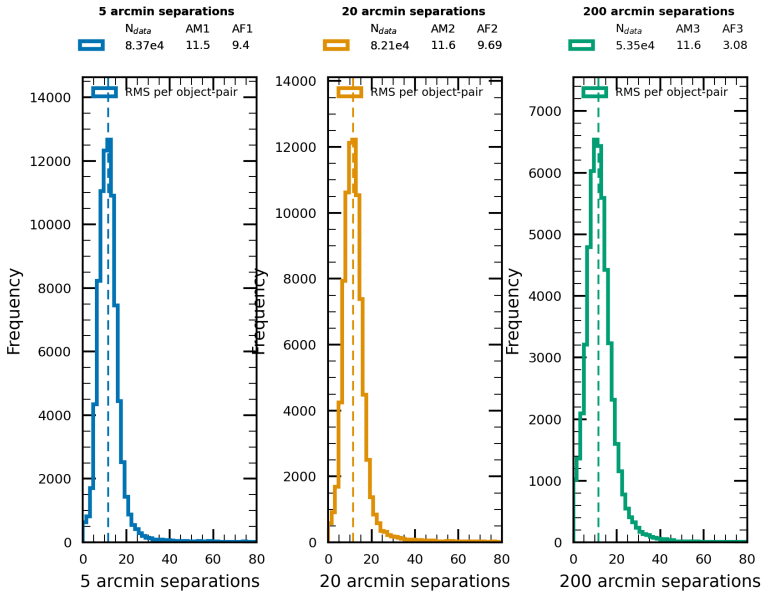

FIGURE 13: Map of the AM1 astrometric repeatability metric across the Science Validation survey region. The majority of the field achieves 10 mas RMS repeatability, consistent with design specifications.

chip-to-chip residuals and systematic trends between ITL and e2v sensors become visible.

The refined camera model is now incorporated into single-frame processing, improving the accuracy of instrumental calibration and the consistency of WCS solutions.

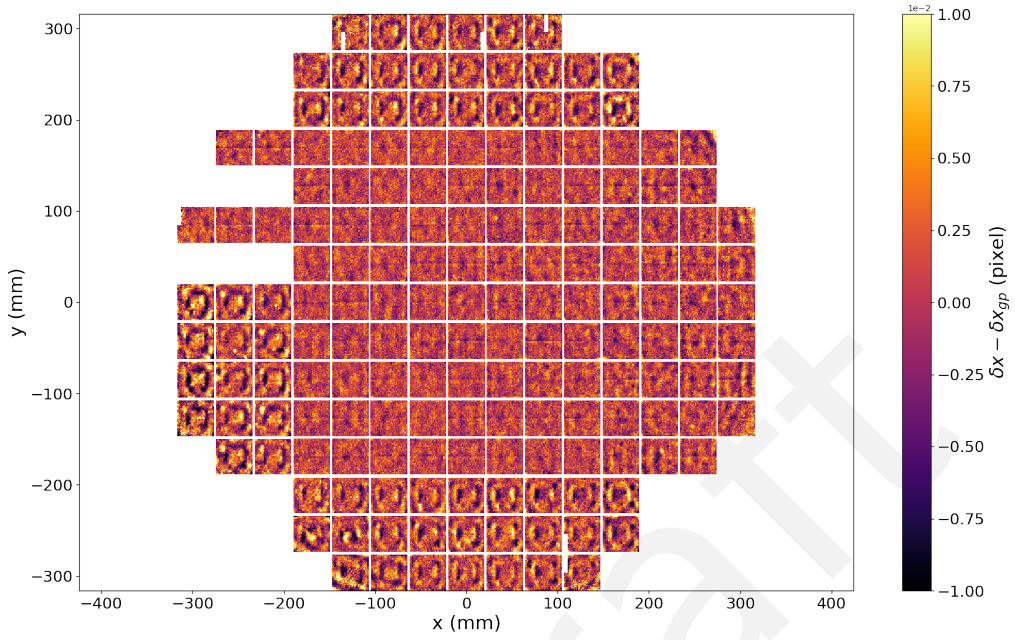

FIGURE 14: Mean astrometric residuals across the focal plane in X (left) and Y (right) directions. The spatial structure is consistent with atmospheric turbulence and small chip-level distortions.

10.1.4 Summary

Astrometric repeatability with LSSTCam currently achieves approximately 10 mas precision, consistent with design specifications in regions with focal-plane-scale dithers. Residuals at the single-visit level are dominated by atmospheric turbulence and are well described by a Gaussian-process model that reduces scatter by about a factor of two. Fine-scale detector distortions are now measurable and are being folded into updated calibration models. A refined, on-sky camera distortion model has been adopted for single-frame processing and continues to improve the overall geometric calibration of the system. Future work will integrate DCR fitting, parallaxes, and the Gaussian-process atmospheric model directly into the global solution for DR1.

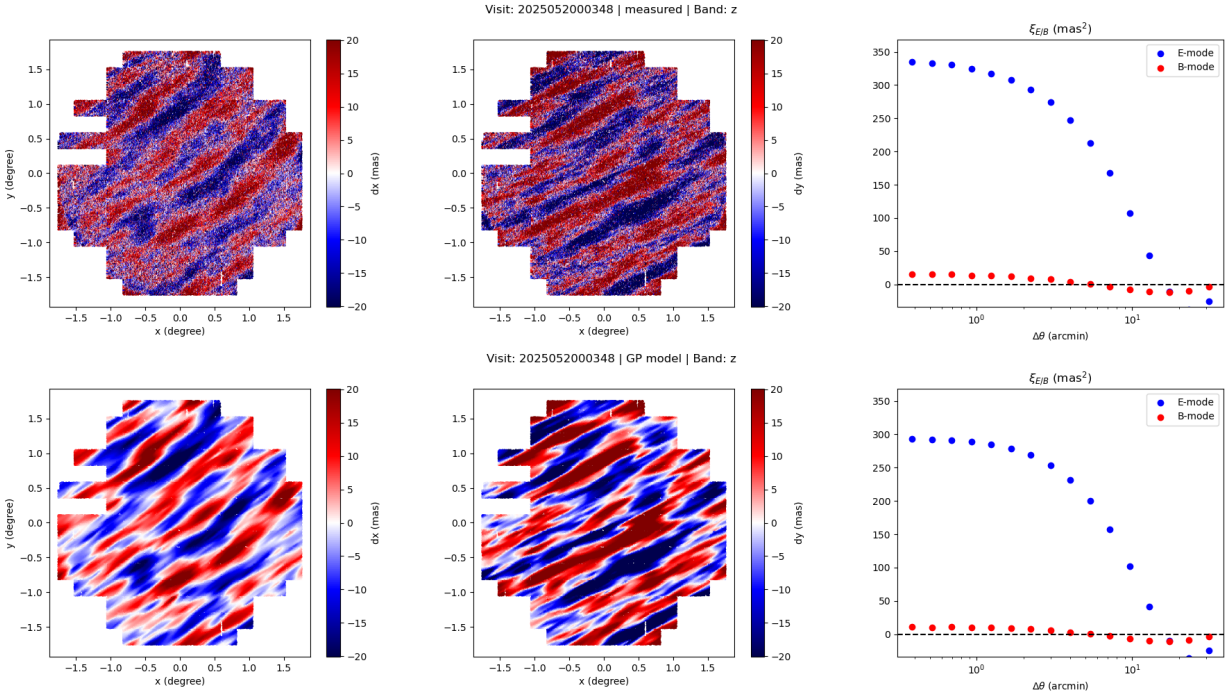

FIGURE 15: Gaussian-process modeling of atmospheric turbulence. The model captures large-scale correlated patterns in the residuals and reduces single-visit astrometric scatter by about 50%.

10.2 Photometry

- Figure: histogram of photometric repeatability for ensemble of visits; panel for each band?
- Figure: illumination correction
- Figure: average photometric residuals in focal plane coordinates for ensemble of visits; maybe a two-panel figure to show full focal plane and an individual detector
- Any other correlations of photometry that are worth exploring further (e.g., residuals w/ respect to stellar color, stellar flux, airmass)

Photometric calibration establishes the flux scale uniformity across the focal plane and over time, providing the foundation for all downstream science measurements. The LSSTCam system now achieves internal photometric repeatability at or below the 5 millimag (mmag) level, consistent with design requirements.

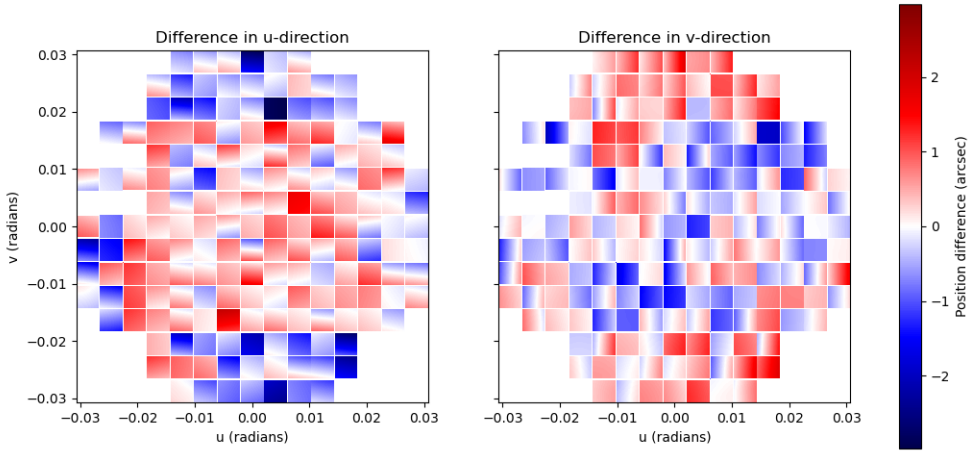

FIGURE 16: Comparison between the pre-commissioning camera model and the astrometry-derived distortion model. Residuals after removing a first-order affine term reveal fine-scale chip-to-chip differences and sensor-dependent trends.

10.2.1 Reference Catalog and Initial Zeropoints

The first stage of the calibration uses the MONSTER reference catalog (Ferguson et al., DMTN-277, DMTN-277), a composite all-sky dataset cross-calibrated from SkyMapper, Pan-STARRS, Gaia XP, and other surveys. Each LSSTCam detector receives an individual zeropoint solution by matching instrumental fluxes to the reference catalog. This per-detector calibration already delivers sub-percent photometric repeatability in the $griz$ bands, as shown in These initial zeropoints are used for prompt processing, which does not include a global calibration step.

10.2.2 Global Forward Calibration

The Forward Global Calibration Method (`fgcmcal`) combines all visits to produce a self-consistent photometric solution that includes illumination and chromatic corrections. This method jointly fits the atmosphere, instrumental throughput, and detector response across the focal plane. The resulting photometric repeatability is 4–5 mmag in all bands ($ugrizy$), meeting the LSST photometric uniformity requirement (Fig. 18).

At this precision, the observed scatter is approaching the limit set by Poisson noise in the stellar measurements themselves. The intrinsic calibration precision is therefore likely closer

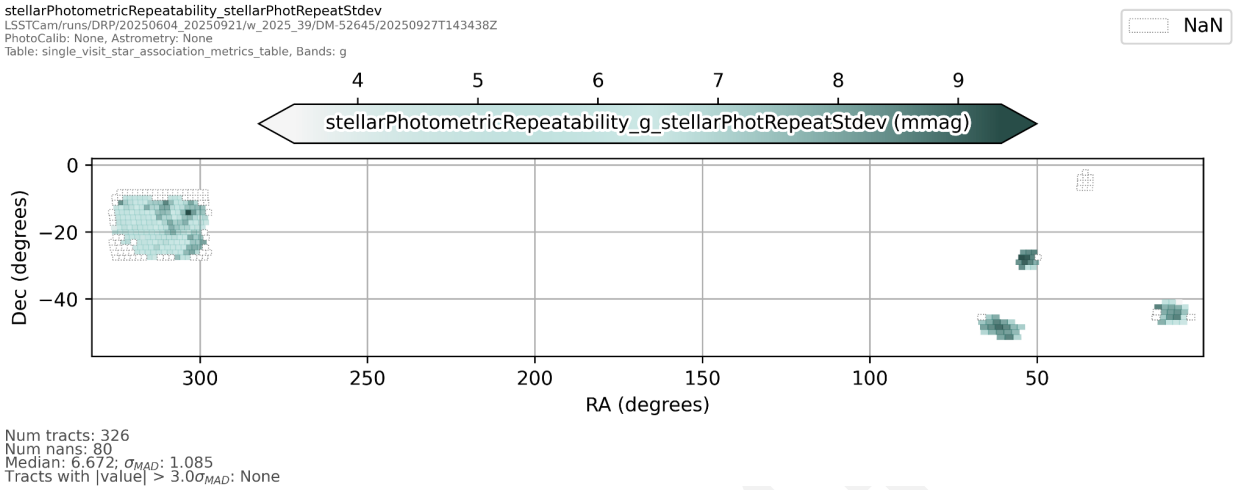

FIGURE 17: Per-detector zeropoint calibration using the MONSTER reference catalog. The preliminary calibration achieves better than 1% repeatability for bright, isolated sources in the $griz$ bands.

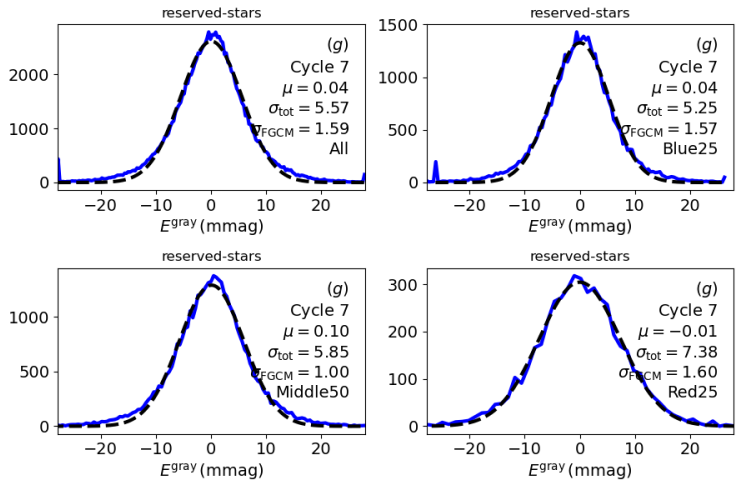

FIGURE 18: Photometric repeatability before and after application of the Forward Global Calibration Method (`fgcmcal`). The global solution achieves 4–5 mmag internal repeatability across all bands.

to the 2 mmag level.

10.3 Chromatic Response Across the Focal Plane

The chromatic response of the LSSTCam focal plane varies with both detector type and filter transmission. The effect is strongest in the g band, where the hybrid focal plane combines ITL and e2v sensors with slightly different quantum efficiency curves. Figure 19 com-

pares the predicted chromatic response—based on laboratory filter scans and detector QE measurements—to the measured on-sky response derived from stellar photometry.

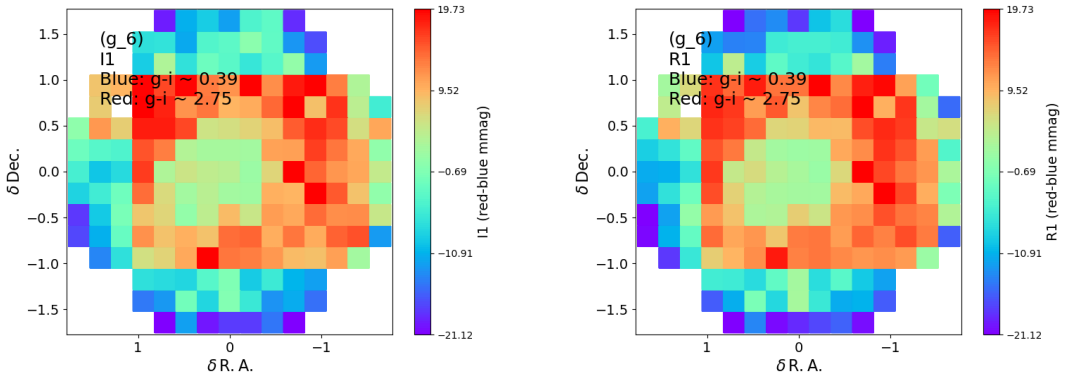

FIGURE 19: Predicted (left) and measured (right) chromatic response across the g-band focal plane. The measured variation is within ± 20 mmag, demonstrating excellent agreement with the predicted response. Accurate modeling of this chromatic structure is critical for maintaining uniformity at the sub-percent level.

The strong correspondence between the measured and predicted patterns indicates that the physical modeling of the detector and filter system is accurate at the level required for precision photometry. Incorporating these chromatic corrections into `fgcmcal` ensures that color-dependent throughput effects are accounted for in the final photometric solution.

10.3.1 Summary

LSSTCam photometric calibration now achieves internal repeatability at or below 5 mmag, comfortably meeting design requirements. Per-detector zeropoints using the MONSTER catalog already reach sub-percent precision, while the global `fgcmcal` solution provides 4–5 mmag repeatability across all bands. Measured chromatic response maps agree closely with predictions, validating the laboratory throughput models and confirming the accuracy of the chromatic correction applied in the pipeline. Future work will focus on refining illumination corrections and incorporating updated reference catalogs for the final DR1 global calibration.

A Acknowledgements

This material is based upon work supported in part by the National Science Foundation through Cooperative Agreements AST-1258333 and AST-2241526 and Cooperative Support Agreements

AST-1202910 and AST-2211468 managed by the Association of Universities for Research in Astronomy (AURA), and the Department of Energy under Contract No. DE-AC02-76SF00515 with the SLAC National Accelerator Laboratory managed by Stanford University. Additional Rubin Observatory funding comes from private donations, grants to universities, and in-kind support from LSST-DA Institutional Members.

B References

[SITCOMTN-005], Claver, C., Bauer, A., Bechtol, K., et al., 2025, *Construction Completeness and Operations Readiness Criteria*, Commissioning Technical Note SITCOMTN-005, NSF-DOE Vera C. Rubin Observatory, URL https://sitcomtn-005.lsst.io/

[LSE-29], Claver, C.F., The LSST Systems Engineering Integrated Project Team, 2017, *LSST System Requirements (LSR)*, Systems Engineering Controlled Document LSE-29, NSF-DOE Vera C. Rubin Observatory, URL https://ls.st/LSE-29

[LSE-30], Claver, C.F., The LSST Systems Engineering Integrated Project Team, 2018, *Observatory System Specifications (OSS)*, Systems Engineering Controlled Document LSE-30, NSF-DOE Vera C. Rubin Observatory, URL https://ls.st/LSE-30

[SITCOMTN-166], Drlica-Wagner, A., Taranto, A., Rodeghiero, G., et al., 2025, *Investigation of the Scratched Tape Scattered Light Artifact at Rubin Observatory*, Commissioning Technical Note SITCOMTN-166, NSF-DOE Vera C. Rubin Observatory, URL https://sitcomtn-166.lsst.io/

[DMTN-277], Ferguson, P.S., Rykoff, E.S., Carlin, J.L., Saunders, C., Parejko, J.K., 2025, *The Monster: A reference catalog with synthetic ugrizy-band fluxes for the Vera C. Rubin observatory*, Data Management Technical Note DMTN-277, NSF-DOE Vera C. Rubin Observatory, URL https://dmtn-277.lsst.io/, doi:10.71929/rubin/2583688

[RTN-011], Guy, L.P., Bechtol, K., Bellm, E., et al., 2025, *Rubin Observatory Plans for an Early Science Program*, Technical Note RTN-011, NSF-DOE Vera C. Rubin Observatory, URL https://rtn-011.lsst.io/, doi:10.71929/rubin/2584021

Ivezić, Ž., Kahn, S.M., Tyson, J.A., et al., 2019, ApJ, 873, 111 (arXiv:0805.2366), doi:10.3847/1538-4357/ab042c, ADS Link

Marchiori, G., De Lorenzi, S., Martinez, J., et al., 2024, In: Marshall, H.K., Spyromilio, J., Usuda, T. (eds.) Ground-based and Airborne Telescopes X, vol. 13094 of Society of Photo-Optical Instrumentation Engineers (SPIE) Conference Series, 1309404, doi:10.1117/12.3018132, ADS Link

[SITCOMTN-173], Pai, A., 2025, *Ghost Impacted Area*, Commissioning Technical Note SITCOMTN-173, NSF-DOE Vera C. Rubin Observatory, URL https://sitcomtn-173.lsst.io/

[SITCOMTN-160], Rodeghiero, G., 2025, *Stray Light Investigation*, Commissioning Technical Note SITCOMTN-160, NSF-DOE Vera C. Rubin Observatory, URL https://sitcomtn-160.lsst.io/

[SITCOMTN-165], Zhou, C., Jeltema, T., von der Linden, A., et al., 2025, *Surface brightness profiles around massive galaxies in LSSTComCam data*, Commissioning Technical Note SITCOMTN-165, NSF-DOE Vera C. Rubin Observatory, URL https://sitcomtn-165.lsst.io/, doi:10.71929/rubin/3000576

C Acronyms

Acronym	Description
ADC	atmospheric dispersion corrector
AST	NSF Division of Astronomical Sciences
AURA	Association of Universities for Research in Astronomy
B	Byte (8 bit)
CBP	Collimated Beam Projector
CCD	Charge-Coupled Device
DCR	Differential Chromatic Refraction
DE-AC02	Department of Energy contract number prefix
DM	Data Management
DMTN	DM Technical Note
DOE	Department of Energy
DP2	Data Preview 2
DR1	Data Release 1
DRP	Data Release Processing
FWHM	Full Width at Half-Maximum

HEALPix	Hierarchical Equal-Area iso-Latitude Pixelisation
HSC	Hyper Suprime-Cam
ISR	Instrument Signal Removal
ITL	Imaging Technology Laboratory (UA)
LED	Light-Emitting Diode
LSR	LSST System Requirements; LSE-29
LSST	Legacy Survey of Space and Time (formerly Large Synoptic Survey Telescope)
LSST-DA	LSST Discovery Alliance
LSSTCam	LSST Science Camera
LSSTComCam	Rubin Commissioning Camera
LVV	LSST Verification and Validation
LWS	Light-Wind Screen
M1	Primary Mirror
M2	Secondary Mirror
M3	Tertiary Mirror
NSF	National Science Foundation
OSS	Observatory System Specifications; LSE-30
PSF	Point Spread Function
PTC	Photon Transfer Curve
Pan-STARRS	Panoramic Survey Telescope and Rapid Response System
QE	quantum efficiency
RMS	Root-Mean-Square
RTN	Rubin Technical Note
SLAC	SLAC National Accelerator Laboratory
SV	Science Validation
TLS	Transport Layer Security
TMA	Telescope Mount Assembly
WCS	World Coordinate System
XP	B or R Photometry (Gaia)